AGU ADVANCING EARTH AND SPACE SCIENCE

Geophysical Research Letters

RESEARCH LETTER
10.1029/2021GL094279

Key Points:

- The fraction of discharge beneath the jam increases with jam resistance
- Backwater rise increases with discharge beneath jam and thus with jam resistance
- Backwater rise is predicted from total discharge, and jam and gap geometry

Supporting Information:

Supporting Information may be found in the online version of this article.

Correspondence to:

E. Follett,
emf@alum.mit.edu

Citation:

Follett, E., Schalko, I., & Nepf, H. (2021). Logjams with a lower gap: Backwater rise and flow distribution beneath and through logjam predicted by two-box momentum balance. *Geophysical Research Letters*, *48*, e2021GL094279. https://doi.org/10.1029/2021GL094279

Received 11 MAY 2021
Accepted 25 JUL 2021

Logjams With a Lower Gap: Backwater Rise and Flow Distribution Beneath and Through Logjam Predicted by Two-Box Momentum Balance

E. Follett[1], I. Schalko[2,3], and H. Nepf[3]

[1]Hydro-environmental Research Centre, School of Engineering, Cardiff University, Cardiff, UK, [2]Laboratory of Hydraulics, Hydrology and Glaciology (VAW), ETH Zurich, Zurich, Switzerland, [3]Department of Civil and Environmental Engineering, Massachusetts Institute of Technology, Cambridge, MA, USA

Abstract Logjams with a gap at the bed form naturally in small channels and are used in engineering practice to maintain river connectivity at base flow. Limited understanding of a jam's effect on backwater rise and flow velocity limits assessment of geomorphic and ecological impacts of natural logjams, design of river restoration interventions, and representation in flood models. The distribution of flow through and beneath the jam satisfies a two-box, momentum-based model constrained by drag generated in the jam, momentum loss in flow through the lower gap, and net pressure force. The model was validated with 68 flume experiments. Backwater rise is predicted from discharge beneath the jam following established models for solid sluice gates. As a result, backwater rise increases with jam resistance, which forces a greater discharge beneath the jam. Below-jam velocity and Shields parameter increased with ratio of friction coefficient to slope and decreasing gap height.

Plain Language Summary Logjams with a lower gap increase river habitat diversity by creating an upstream backwater of slower, deepened water promoting sediment capture, with a region of faster flow underneath the jam aiding flushing of fine particles from clogged gravels and local pool generation suitable for fish refuge. Prediction of the flow distribution between the jam and lower gap and rise in upstream water depth from the measured gap height and shape of logs and fine material (branches and leaves) is necessary to understand the impact of logjams on geomorphic diversity and habitat complexity of small streams, which form a majority of river networks by length, to improve design of river restoration projects, and to assess flood risk. Using experimental measurements in a hydraulic flume, we demonstrate that the upstream water depth and flow distribution between the jam and gap regions can be predicted with a sluice gate model together with the drag generated by the jam. Relative flow velocity underneath the jam and sediment transport potential increased with ratio of channel friction to channel steepness and decreasing gap height.

1. Introduction

Instream large wood (LW, defined as logs with diameter ≥ 0.1 m and length ≥ 1.0 m, Keller & Swanson, 1979; Wohl & Jaeger, 2009) increases spatial heterogeneity of flow and sediment transport, providing improved habitat complexity with recognized benefits to fish and invertebrate populations (Bouwes et al., 2016; Faustini & Jones, 2003; L'Hommedieu et al., 2020; Schalko et al., 2018, 2021; Wohl et al., 2016). Wood presence increases the average roughness of stream reaches (Follett et al., 2020; Hankin et al., 2020; Shields & Gippel, 1995), enhancing channel-floodplain connectivity. Recent restoration interventions have sought to increase the presence of instream LW through woodland management and installation of engineered logjams (Bennett et al., 2015; Burgess-Gamble et al., 2017; Dadson et al., 2017; Gallisdorfer et al., 2014; Ismail et al., 2021). Under some conditions, LW aids natural flood management objectives by improving water storage and floodplain infiltration, but LW also poses a flood hazard, especially at instream structures such as bridges or weirs (Schalko et al., 2018). Knowledge gaps surrounding the underlying physical processes by which LW affects in-channel flow, floodplain inundation and sediment transport have led to calls for evidence (Dadson et al., 2017; Wohl et al., 2016) and process-based theoretical development (Wohl et al., 2005) to improve the design and assessment of river restoration interventions using LW.

Figure 1. Engineered jam with lower gap installed in Pig Brook near Shipston-on-Stour, England, UK. Water depth upstream of jam has risen to bankfull level. Flow direction from right to left. Photo credit: Mr Geoff Smith/Shipston Area Flood Action Group.

Logjams may form spontaneously at instream obstructions or be installed as engineered structures through flood management and river restoration projects. In large channels capable of transporting LW, natural logjams are commonly initiated and stabilized by a key log (Abbe & Montgomery, 2003; Davidson et al., 2015; Manners & Doyle, 2008; Nakamura & Swanson, 1994; Wallerstein & Thorne, 1996). In narrow channels with bankfull width B_{bf} less than LW length, logjams with a lower gap may form as additional wood pieces accumulate upstream of a key log supported by both channel banks (Abbe & Montgomery, 2003). Engineered logjams are typically created from multiple smaller wood pieces, often sourced locally to the installation site (Burgess-Gamble et al., 2017), and are commonly located at smaller, narrow ($B_{bf} < 3$ m) streams (Riley et al., 2018). In the UK and EU, structures often span the upper channel with a gap between the channel bed and structure lower edge (Figure 1) in order to allow fish passage at base flow (Dodd et al., 2016) and maintain quality of river continuity assessed as part of EU Water Framework Directive requirements (Burgess-Gamble et al., 2017; Dodd et al., 2016; Forbes et al., 2015).

Logjams create an upstream area of slower, deepened water, increasing channel-floodplain connectivity and deposition of sediment and fine particles (Bilby, 1981). The increase in upstream water depth, or backwater rise, generated by channel-spanning logjams has recently been described using a combination of momentum and energy constraints (Follett et al., 2020). Jams with a gap at the bed have been previously modeled as sluices with an empirically determined permeability coefficient (Hankin et al., 2020; Leakey et al., 2020). In this paper we consider flow through the gap using established sluice gate models (Chow, 1959; Henderson, 1966; Malcherek, 2018), together with drag generated by the group of logs in the jam region, which is represented by an adaptation of the law for drag in canopies (Follett et al., 2020). A two-box, momentum-based model is presented, which predicts the distribution of flow between the jam and gap and a physically based stage-discharge relationship for logjams with a gap at the bed.

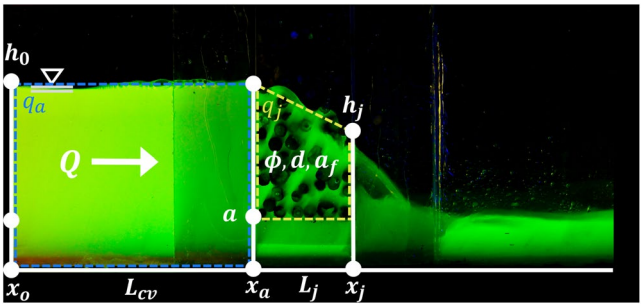

Figure 2. Side view of experimental setup. Discharge Q partitions between the jam ($z > a$) and lower gap ($z = 0$ to a) regions in a rectangular open channel of width B. The porous logjam had length L_j, solid volume fraction ϕ, large wood (LW) diameter d, and spatial average frontal area density a_f. Flow direction indicated by white arrow. Upstream water depth h_0 was measured $L_{cv} = 1$ m upstream of jam leading edge. Discharge through the jam q_j calculated for yellow control volume extending from $x = x_a$ to x_j and $z = a$ to h_0, h_j (Follett et al., 2020). Discharge through the gap q_a estimated for blue control volume $x = x_0$ to x_a and $z = 0$ to h_0, accounting for discharge through the jam.

2. Methods

2.1. Experimental Materials and Methods

Predictions of both the backwater rise and discharge partitioning between the porous jam and gap at the bed were tested with 68 experiments in an 0.3 m wide, 10 m long glass-walled flume at Cardiff University (UK) with bed slope $S = 0.001$. A table of experimental parameters is publically available (Follett, 2021). A diagram of the flume setup is available as supporting information. Cylindrical logs were used to construct porous jams with a lower gap extending from the flume bed to the jam lower edge over vertical distance $z = 0$ to a (Figure 2). Logs were held in place using a set of thin acrylic plates attached to the flume sidewalls. The plates were observed to have no measurable effect on the water surface profile in tests with no jam present. A flap gate at the downstream end of the flume was adjusted to obtain uniform flow depth with no jam present. Measurements with no jam present with $Q = 0.0038 - 0.028\text{m}^3$ / and $h = 0.03 - 0.11$ m indicated that friction coefficient $C_f = 0.0025 - 0.0015$, and C_f was interpolated from measured values in later analysis. The effect of jam presence on upstream and downstream water depth was measured for discharge $Q = 0.0019 - 0.033$ m^3/s, jam length $L_j = 0.025 - 0.2$ m, LW diameter $d = 0.016 \pm 0.003$ m and solid volume fraction $\phi = 0.51$. Solid volume fraction was found by dividing measured solid wood volume by measured jam volume (Schalko et al., 2018). The height of the

gap above the flume bed a and height of water exiting the jam h_j above the bed were measured with a ruler placed along the flume sidewall. Flow depth 1 m ($x = L_{cv}$) upstream of the jam h_0 was measured with a point gauge. Depth-average time-mean longitudinal velocity (U) and discharge ($Q = UBh$) were found for fully developed, turbulent flow from acoustic Doppler velocimeter (Nortek Vectrino) measurements observed at $z = 0.6h$ along the channel centerline, with recordings taken for 5 min (25 Hz) and time averaged. Silica seeding particles (Sphericell 110P8, Potters Europe, Barnsley), and fluorescein and rhodamine water tracing dye (Cole-Parmer, St. Neots) were used to provide reflecting surfaces for ADV measurement, define the water surface profile, and aid visualization of flow in the gap region, respectively.

Velocity in the lower gap U_a was estimated from visual observation of the number of digital video frames (n, sampled at 50 frames s^{-1}) required for the leading edge of injected rhodamine dye to traverse L_j for 21 experiments. At least three observations were made per experimental case. Uncertainty was quantified based on limitations in the framing rate (minimum detected $U_a = 50L_j / n$, resolution $\frac{1}{n(n-1)}50L_j$). Longitudinal dispersion of rhodamine was estimated to decrease measured U_a by 0.02% and was neglected. Because of these limitations, U_a was not recorded in cases for which the dye plume required less than 2 frames to traverse L_j.

3. Theory

3.1. Conservation of Momentum for Solid Sluice Gates

We first consider conservation of momentum for solid, vertical sluice gates extending from $z = a$ to the water surface in a rectangular open channel with slope S and width B. Conservation of momentum (Malcherek, 2018) was considered for the blue control volume in Figure 2 extending vertically from $z = 0$ to $z = h_0$ and over longitudinal distance L_{cv} from the gate upstream edge ($x = x_a$) to a distance upstream ($x = x_0$) where the influence of near-gate water surface set up is not present and $z = h_0$,

$$\underbrace{F_p}_{\text{net pressure force}} + \underbrace{\rho Bq^2\left(\frac{1}{h_0} - \frac{\beta_a}{a}\right)}_{\text{net change in momentum}} - \underbrace{\frac{1}{2}\rho C_f U^2 L_{cv}\left(B + 2h_0\right)}_{\text{shear stress at bed and sidewalls}} + \underbrace{\rho g B h_0 L_{cv} S}_{\text{bed slope}} = 0, \tag{1}$$

with momentum correction factor $\beta_a = 1$ for flow under the gate ($h_0 < a$) and for high relative submergence depths ($h_0 / a \gg 1$), and $\beta_a > 1$ for intermediate relative submergence (Malcherek, 2018).

Following models for solid sluice gates, the pressure force in the region upstream of the lower gap ($z = 0$ to a) was assumed to be hydrostatic at a distance L_{cv} upstream of the gate ($x = x_0, z = h_0$),

$$F_{p0} = \frac{1}{2}\rho g B a(2h_0 - a), \tag{2}$$

and to follow a quadratic profile just upstream of the gate at $x = x_a$, so that

$$F_{pa} = Ba\left[\frac{2}{3}p_b(x_a) - \frac{1}{6}\rho g a\right], \tag{3}$$

(Malcherek, 2018), with bottom pressure p_b at $x = x_a$. Note that between $z = a$ and h_0 the net hydrostatic pressure force is the same on both faces of the control volume, so that this region was excluded from the force balance. The bottom pressure along the centerline of a channel with a solid sluice gate was measured by Roth & Hager (1999), from which Malcherek (2018) defines the bottom pressure at the sluice gate, $p_b(x_a) = \rho g(0.5h_0 + 0.5a)$. Combining Equation 2 and Equation 3 yields the following expression for the net pressure force in Equation 1,

$$F_p = F_{p0} - F_{pa} = C_{p0}\rho g B a(h_0 - a) \tag{4}$$

with $C_{p0} = 2 / 3$. For the experiments conducted, maximum shear stress at the bed and sidewalls was estimated with gap velocity U_a. The estimated bed shear stress and weight of water on bed slope S were much smaller than the net pressure force and net change in momentum for cases with $h_0 > a$ (0.041 ± 0.06 (σ) when $h_0 / a > 1.1$). For cases in which the water depth was less than the gap height ($h < a$), the net pressure force and net change in momentum are zero, with flow in an unobstructed, wide rectangular open channel

given by the balance between shear stress at the bed and weight of water on bed slope S, $q^2 = \frac{S}{C_f} g h^3$ (Chow, 1959; Henderson, 1966; Julien, 1998). For simplicity and correspondence with wide channels, the contribution of shear stress at the sidewalls was excluded from later analysis with C_f for experimental data fit to uniform flow in a wide channel. Neglecting the effect of bed slope and bed shear stress, and defining the net pressure force on the control volume as F_p in Equation 1, we obtain a simplified stage-discharge relationship for solid gates (Malcherek, 2018),

$$\rho B q^2 \left(\frac{1}{h_0} - \frac{\beta_a}{a} \right) + F_p = 0, \tag{5}$$

which, with rearrangement, is seen to be analogous to an energy-based Bernoulli approach with C_{dg} as discharge coefficient (Aigner & Bollrich, 2015; Chow, 1959; Henderson, 1966; Malcherek, 2018),

$$q^2 = C_{p0} g a^2 h_0 \left(\frac{\frac{a}{h_0} - 1}{\frac{a}{h_0} - \beta_a} \right) \approx 2 C_{dg}^2 g a^2 h_0. \tag{6}$$

Elevated momentum coefficient β_a in the gap, associated with nonuniform vertical velocity distribution (Chow, 1959) has previously been described with a Rayleigh-Weibull distribution (Equation 11 in Malcherek, 2018). Varying β_a is analogous to varying discharge coefficient C_{dg} in an energy-based approach, with C_{dg} empirically observed to vary with a / h_0 [$C_{dg} = \frac{C_c}{1 + C_c \frac{a}{h_0}}$ (Henderson, 1966)]. Relative submergence depths of primary interest for logjams lie in the transitional region ($h_0 / a < 10$) with elevated β_a (Malcherek, 2018). To ensure a smooth transition between unobstructed uniform flow when water depth is below the jam lower edge ($h_0 < a$) and low relative submergence depths ($h_0 / a \approx 1$), we define β_a following the semiempirical functional form $C_p = \frac{C_{p0}}{(1 + C_b \frac{a}{h_0})}$ used for solid gates, with bottom coefficient $C_b = \frac{C_{p0} C_f}{S} - 1$, which matches uniform flow when $h_0 / a = 1$. This requires,

$$\beta_a = 1 - C_b \frac{a}{h_0} \left(\frac{a}{h_0} - 1 \right). \tag{7}$$

The momentum balance of Equation 5 with β_a given by Equation 7 was used for later analysis of logjams.

3.2. Conservation of Momentum for Jams With a Lower Gap

Water approaching a jam with a lower gap partitions between the porous jam and the gap beneath the jam. Flow exiting the jam adopted an elevated height $h_j > a$ (Figure 2) similar to previous observations of flow through channel-spanning jams without a lower gap (Follett et al., 2020). Negligible exchange of flow between the jam and gap sections was visually observed from injections of rhodamine dye. The fraction of total unit discharge $q = Q / B$ passing through the jam ($z > a$) was defined as J, with unit discharge $q_j = Jq$ passing through the jam and $q_a = (1 - J)q$ passing through the gap. To predict the redistribution of flow between the jam and gap and the backwater rise, we considered a two-box momentum model and mass conservation, $q = q_j + q_a$. Loss of momentum in the gap was assumed to be the same as for a solid sluice, which was balanced by a pressure force F_p as in Equation 5, that is,

$$q_a = \left(C_p g a^2 h_0 \right)^{1/2}. \tag{8}$$

Note that this neglects additional losses that occur along the length of the gap, an assumption which degrades as the jam length increases. Within the jam, conservation of momentum reduces to a balance of hydrostatic pressure and drag on jam elements, which provides a relation between the upstream water depth (h_0) and discharge through the jam (q_j) (Equation 6 in Follett et al., 2020),

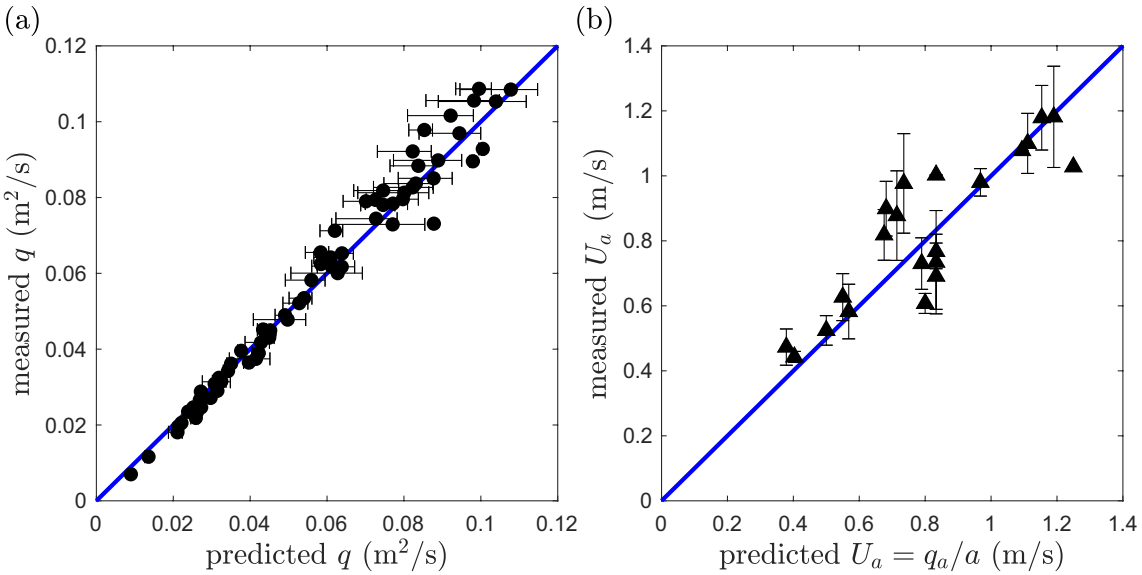

Figure 3. (a) Measured unit discharge compared to predicted unit discharge (Equation 11; black filled circles). Line of equality $y = x$ is shown in solid blue. Error due to observed variation in $C_A = 22 \pm 9$ measured from 23 measurements of four repeat channel-spanning jams constructed using the same set of logs. (b) Measurements of spatial average velocity in the lower gap ($z = 0$ to a) $U_a = q_a / a$ (Equation 8; black filled triangles). Line of equality $y = x$ is shown in solid blue.

$$h_0 - a = \sqrt{3}\left(\frac{C_A q_j^2}{2g}\right)^{1/3} . \tag{9}$$

The drag within the jam is characterized by the jam accumulation factor $C_A = \frac{L_j C_D a_f}{(1-\phi)^3}$ (Follett et al., 2020) with spatial average frontal area density a_f. By rearrangement of Equation 9, the discharge passing through the jam layer is

$$q_j = \left[\frac{2g\left(h_0 - a\right)^3}{3\sqrt{3}C_A}\right]^{1/2} \tag{10}$$

The total discharge passing through the section is then the sum of Equation 10 and Equation 8,

$$q = \left[\frac{2g\left(h_0 - a\right)^3}{3\sqrt{3}C_A}\right]^{1/2} + \left[\frac{C_{p0}}{\left(1 + C_b\frac{a}{h_0}\right)} g a^2 h_0\right]^{1/2} , \tag{11}$$

from conservation of mass between the jam and gap regions.

4. Results and Discussion

4.1. Flow Distribution Beneath and Through Logjam

Measured unit discharge from 68 experiments agreed within uncertainty (Figure 3a) with predictions from Equation 11 using $C_A = 22 \pm 9$ which was based on 23 measurements of four repeat channel-spanning jams constructed using the same set of logs, $a = 0.018 - 0.1$ m, $L_j = 0.025 - 0.2$ m, and $q = 0.0019 - 0.032$ m^2 / s. The linear fit between measured and predicted q had a slope 1.02 with 95% CI (1.00, 1.03) found from multiple linear regression (Matlab *regress*). The prediction $U_a = q_a / a$, with q_a predicted from Equation 8, was validated with measurements of average velocity in the gap U_a (Figure 3b). The linear fit be-

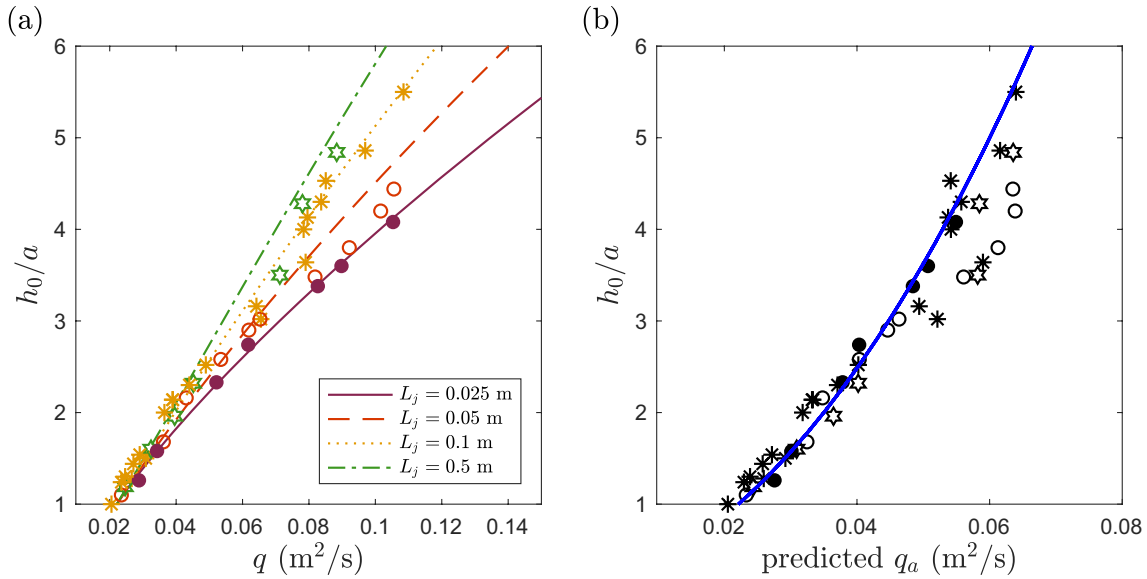

Figure 4. (a) Measured upstream water depth relative to lower gap height h_0 / a versus measured unit discharge qm^2 / s for porous wood jams with lower gap height a = 0.05 m and varying L_j = 0.025,0.05,0.1,0.2 m, respectively shown by red filled circles, orange open circles, yellow asterisks, and green stars. Predicted h_0 / a versus q (Equation 11) for varying L_j shown with red solid, orange dashed, yellow dotted, and green dash-dotted lines, respectively. Effect of varied $L_j \sim C_A$ ($C_A = L_j C_D a_f / (1-\phi)^3$, Follett et al., 2020) became more pronounced with increasing discharge through the jam. (b) Measured h_0 / a compared to unit discharge through the lower gap found from conservation of mass $q_a = q - q_j$ with measured q and q_j predicted by Equation 10. Jams with varying L_j = 0.025,0.05,0.1,0.2 m are respectively shown with black filled circles, open circles, asterisks, and stars. Predicted q_a (Equation 8) for varying h_0 / a shown in solid blue.

tween measured and predicted U_a had a slope 0.97 with 95% CI (0.91, 1.04) found from multiple linear regression (Matlab regress) for 21 experiments with $C_A = 22 \pm 9$, a = 0.018 – 0.1 m, L_j = 0.025 – 0.200 m, and q = 0.006 – 0.03 m^2/s. The good agreement between Equation 8 and measured U_a indicated that the neglect of losses along the gap was appropriate for the jam lengths considered in this study.

4.2. Effect of Varying Logjam Length

In the field, jam length and density may vary over time due to accumulation or loss of wood pieces and fine material (Schalko et al., 2018). Changes to L_j alter the jam accumulation factor C_A ($C_A \sim L_j$), increasing resistance of the jam. The effect of jam length was tested with jams with varying L_j = 0.025, 0.05, 0.1, 0.2 m and constant gap height a = 0.05 m (Figure 4). Measured h_0 / a and q are shown with red solid circles, orange open circles, yellow asterisks, and green stars, respectively for increasing L_j. Predicted q for varying h_0 / a (Equation 11) is shown with red solid, orange dashed, yellow dotted and green dash-dot lines, respectively for increasing L_j. For constant q, increasing jam length was associated with increasing upstream water depth h_0 (Figure 4a). The relationship between h_0 / a and q_a did not depend on L_j, illustrating that flow through the gap was not a function of jam characteristics and was consistent with solid sluice gate predictions (Figure 4b; predicted solution from Equation 8 shown with solid blue line).

4.3. Effect of Gap Height on Backwater Rise and Bed Shear Stress Relative to Unobstructed Bankfull Flow

In order to compare the effect of logjams installed in a river channel to an unobstructed channel with bankfull depth H_{bf} and bankfull unit discharge q_{bf}, we consider nondimensional discharge $\hat{q}$ scaled with unobstructed bankfull unit discharge ($\hat{q} = q$ / q_{bf}), bankfull channel depth ($\hat{h} = h_0$ / H_{bf}), and g ($\hat{g} = 1$). Bankfull discharge occurs on average every 1.5 – 2 years in unregulated channels and is associated with the highest in-channel velocity and Shields parameter (Mount, 1995). For flow in channels with median sediment di-

ameter D_{s50}, C_f was based on a logarithmic profile of longitudinal velocity $C_f = (5.75log_{10}(2H_{bf} / D_{s50}))^{-2}$ (Julien, 2010). Because variation of C_f due to flow acceleration underneath the jam and confined gap height are not known, C_f was assumed to equal the value at bankfull depth as a first estimate, and the effect of the logjam was considered only for relative gap heights $\hat{a} = a / H_{bf} > 0.2H_{bf}$. Normalizing Equation 11 with the scales for bankfull flow,

$$\hat{q} = \left[\frac{C_f}{S}\frac{2\hat{g}(\hat{h}-\hat{a})^3}{3\sqrt{3}C_A}\right]^{1/2} + \left[\frac{C_f}{S}\frac{Cp_0}{\left(1+C_b\frac{\hat{a}}{\hat{h}}\right)}\hat{g}\hat{a}^2\hat{h}\right]^{1/2} \quad (12)$$

with dimensionless unit discharge through the jam and lower gap sections respectively given by $\widehat{q_j} = q_j / q_{bf}$ and $\widehat{q_a} = q_a / q_{bf}$. The dimensionless unit discharge $\hat{q}$, ratio of dimensionless unit discharge through the jam and lower gap sections $\widehat{q_j} / \widehat{q_a}$, relative mean longitudinal velocity in the gap relative to mean bankfull velocity in an unobstructed channel $U_a / U_{bf} = \widehat{q_a} / \hat{a}$, and relative Shields parameter $\tau_{*a} / \tau_{*bf} = (u_{*a} / u_{*bf})^2 \approx \left(U_a / U_{bf}\right)^2$ (Julien, 2010) were examined for a porous jam with $C_A = 22$ relative to an unobstructed bankfull channel ($\hat{h} = 1$) and varying dimensionless lower gap height $\hat{a} = 0.2 - 1$ for four UK river channels with reported S, H_{bf}, D_{s50} (Dixon, 2016; Hey & Thorne, 1986) and two hypothetical river channels with predicted D_{s50} based on relations describing bankfull geometry of single-thread gravel rivers (Parker et al., 2007) (Figure 5). Curves B, C and E respectively represent the Wylye at Norton Bavant ($S = 0.001572$, $D_{s50} = 0.0174$ m, $H_{bf} = 1.20$ m), Usway Burn at Shillmoor ($S = 0.008479$, $D_{s50} = 0.1133$ m, $H_{bf} = 1.11$ m), and Chittern at Codford [$S = 0.001935$, $D_{s50} = 0.0232$ m, $H_{bf} = 1.17$ m] (Hey & Thorne, 1986). Curve F represents a fourth-order tributary of the Lymington River within the Highland Water, New Forest National Park ($S = 0.005$, $D_{s50} = 0.029$ m, $H_{bf} = 1.3$ m; Dixon, 2016). Curves A and D respectively represent predicted $D_{s50} = 0.015, 0.21$ m (Parker et al., 2007) for channels with $S = 0.001, 0.01$ and $H_{bf} = 1.2$ m, respectively.

The introduction of a jam with a gap at the bed increased water depth upstream of the barrier relative to unobstructed flow (Figure 5a), so that bankfull water depth upstream of the jam was achieved at progressively decreasing $\hat{q}$ with decreasing $\hat{a}$. The fraction of discharge passing through the jam, relative to the lower gap, increased with decreasing $\hat{a}$ (Figure 5b). Because flow frequency is inversely related to water depth, decreasing gap height increases the frequency at which upstream bankfull inundation would be expected to occur. The relative discharge required to generate bankfull depth upstream of the jam decreased with $\hat{a}$ and C_f / S (Equation 12), with $C_f / S = 6.2, 4.2, 3.9, 2.7, 2.1, 1.6$ respectively for curves A–F. Mean velocity in the lower gap when the upstream depth was at bankfull level, relative to bankfull velocity in an unobstructed channel, increased with C_f / S and decreasing $\hat{a}$ (Figure 5c). Similarly, relative Shields parameter τ_{*a} / τ_{*bf} increased with C_f / S and decreasing $\hat{a}$ due to the dependence on $\left(U_a / U_{bf}\right)^2$ (Figure 5d). Because q_a is directly related to upstream water depth (Figure 4b and Equation 8) but not jam resistance, the curves in Figure 5 do not change with C_A. Sediment diameter in unregulated rivers falls near the critical Shields parameter τ_{*c} associated with onset of sediment motion for bankfull flow (García, 2000; Mount, 1995). Sediment motion underneath the jam would be expected to occur when $\tau_{*a} / \tau_{*bf} > 1$, with the likelihood and potential extent of sediment transport increasing with τ_{*a} / τ_{*bf}. The predicted trend in bed shear stress (Figure 5c) was consistent with prior experimental observations (Follett & Wilson, 2020) that the extent of sediment transport increased with decreasing gap height. Further research is required to understand the variation of C_f in the lower gap from the estimated bankfull value. Prior observations of sediment transport under solid gates (Follett & Wilson, 2020) indicated that higher bulk velocity was required to initiate sediment motion when the gap height approached sediment diameter. Improved understanding of the effects of jams on sediment transport potential aids design choice of gap height to achieve varying management outcomes, ranging from increased sediment retention to the desire to promote flushing of sediment from clogged gravels and generation of local scour pools to provide deepened, cooler fish refuge in summer months.

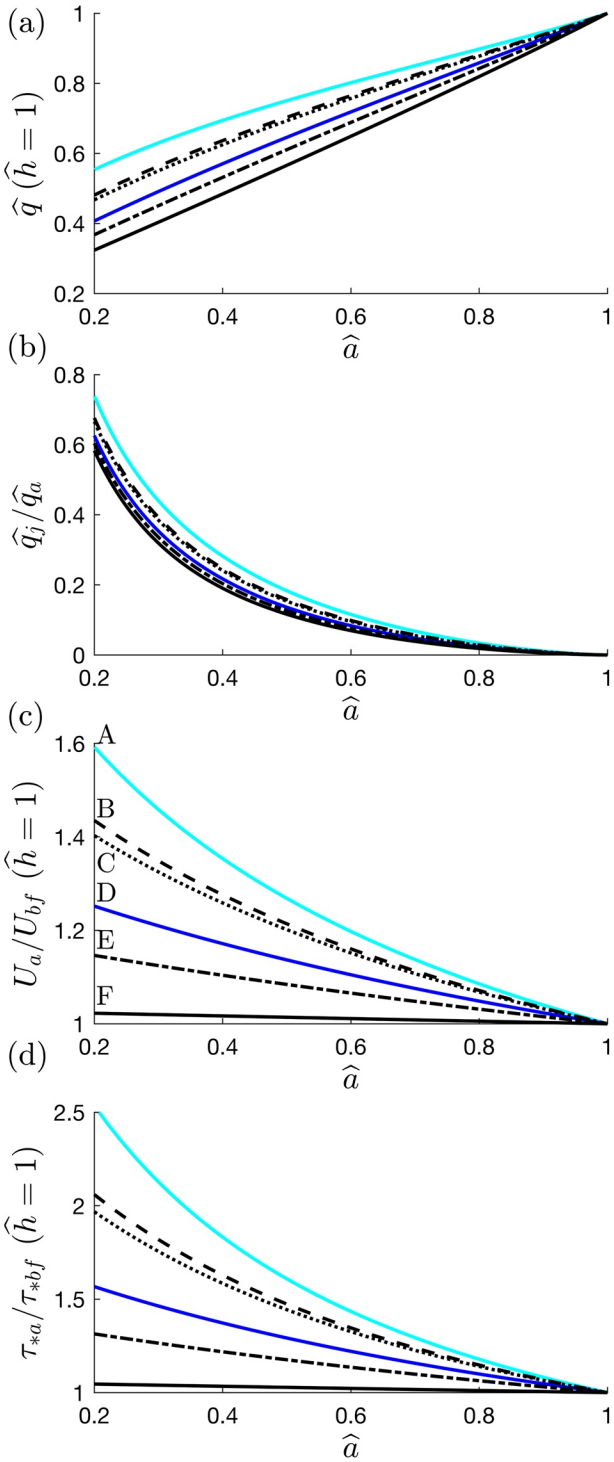

Figure 5. (a) Dimensionless discharge through a channel containing a logjam with lower gap ($C_A = 22$) relative to bankfull discharge in an unobstructed channel ($\hat{q} = q / q_{bf}$) when water depth upstream of the jam is equal to bankfull channel depth ($\hat{h} = h_0 / H_{bf} = 1$) with varying dimensionless gap height relative to bankfull channel depth ($\hat{a} = a / H_{bf} = 0.2 - 1$). Curves A–F respectively represent decreasing ratio of channel friction coefficient to slope, $C_f / S = 6.2, 4.2, 3.9, 2.7, 2.1, 1.6$. (b) Ratio of dimensionless discharge through the jam and lower gap sections. (c) Predicted velocity in the lower gap relative to unobstructed bankfull velocity U_a / U_{bf} when $\hat{h} = 1$ and $\hat{a} = 0.2 - 1$. (d) Predicted Shields parameter underneath jam relative to the Shields parameter in an unobstructed bankfull channel τ_{*g} / τ_{*bf} with $\hat{h} = 1$ and $\hat{a} = 0.2 - 1$. Curves B, C and E (black dashed, dot, and dash-dotted lines) respectively represent S, H_{bf}, D_{s50} measured for the Wylye at Norton Bavant, Usway Burn at Shillmoor, and Chittern at Codford (Hey & Thorne, 1986). Curve F (solid black line) represents measured S, H_{bf}, D_{s50} for a fourth-order tributary of the Lymington River within the Highland Water, New Forest National Park (Dixon, 2016). Curves A and D (cyan and blue solid lines) respectively represent predicted D_{s50} (Parker et al., 2007) for channels with $S = 0.001, 0.01$ and $H_{bf} = 1.2$ m, respectively.

5. Conclusion

Logjams with a lower gap form naturally in narrow channels for which wood falling across the channel is supported by the channel banks (Abbe & Montgomery, 2003) and are commonly used as engineered logjam designs in natural flood management and river restoration projects. The backwater rise and velocity beneath the jam are key factors in determining the ecologic, geomorphic and flood risk impact of a jam. The backwater rise and velocity beneath the jam both increase with increasing jam drag and decreasing gap height. This study provided a prediction of upstream backwater rise and velocity beneath the jam as a function of total discharge and jam geometric features, providing a way to represent jams in numerical flood models and to improve the design and assessment of river restoration and natural flood management projects. This approach allows representation of logjams with a lower gap in a flood model or network analysis (Hankin et al., 2020; Leakey et al., 2020; Persi et al., 2019; Ruiz Villanueva et al., 2014). Prediction of flow distribution and backwater rise due to logjams with a lower gap allows improved design of river restoration interventions that enable river continuity at base flow and achieve varying management goals including fish passage, flood risk, upstream sediment retention, and generation of pools suitable for fish refuge in summer months.

Data Availability Statement

Data sets for this research are available in (Follett, 2021) (CC BY 4.0).

Acknowledgments
The first author has received funding from the Royal Academy of Engineering's Research Fellowships program and the European Regional Development Fund through the Welsh Government Sêr Cymru program 80762-CU-241. The second author was funded by the Swiss National Science Foundation (SNSF) Early Postdoc Mobility Fellowship project No. 184263. Discussion and photo contribution by the Shipston Area Flood Action Group and Environment Agency West Midlands, and assistance in constructing experimental apparatus by Mr Steven Rankmore (Cardiff University) are gratefully acknowledged.

References

Abbe, T., & Montgomery, D. (2003). Patterns and processes of wood debris accumulation in the Queets river basin, WA. *Geomorphology*, *51*, 81–107. https://doi.org/10.1016/S0169-555X(02)00326-4

Aigner, D., & Bollrich, G. (2015). *Handbuch der hydraulik: Für wasserbau und wasserwirtschaft*. Beuth Verlag.

Bennett, S., Ghaneeziad, S., Gallisdorfer, M., Cai, D., Atkinson, J., Simon, A., & Langendoen, E. (2015). Flow, turbulence and drag associated with engineered log jams in a fixed-bed experimental channel. *Geomorphology*, *248*, 172–184. https://doi.org/10.1016/j.geomorph.2015.07.046

Bilby, R. (1981). Role of organic debris dams in regulating the export of dissolved and particulate matter from a forested watershed. *Ecology*, *62*, 1234–1243. https://doi.org/10.2307/1937288

Bouwes, N., Weber, N., Jordan, C. E., Saunders, W. C., Tattam, I. A., & Volk, C., et al. (2016). Ecosystem experiment reveals benefits of natural and simulated beaver dams to a threatened population of steelhead (*Oncorhynchus mykiss*). *Scientific Reports*, *6*, 28581. https://doi.org/10.1038/srep28581

Burgess-Gamble, L., Ngai, R., Wilkinson, M., Nisbet, T., Pontee, N., Harvey, R., & Quinn, P. (2017). *Working with natural processes - evidence directory*. (Technical Report No. SC150005). Bristol: Environment Agency, Horizon House.

Chow, V. (1959). *Open-channel hydraulics*. London: McGraw-Hill Book Company.

Dadson, S., Hall, J., Murgatroyd, A., Acreman, M., Bates, P., Beven, K., et al. (2017). A restatement of the natural science evidence concerning catchment-based 'natural' flood management in the UK. *Proceedings of the Royal Society A*, *473*(2199), 20160706. https://doi.org/10.1098/rspa.2016.0706

Davidson, S. L., Mackenzie, L. G., & Eaton, B. C. (2015). Large wood transport and jam formation in a series of flume experiments. *Water Resources Research*, *51*(12), 10065–10077. https://doi.org/10.1002/2015WR017446

Dixon, S. (2016). A dimensionless statistical analysis of logjam form and process. *Ecohydrology*, *9*, 1117–1129. https://doi.org/10.1002/eco.1710

Dodd, J., Newton, M., & Adams, C. (2016). *The effect of natural flood management in-stream wood placements on fish movement in Scotland*. (Technical Report No. CD2015_02). Aberdeen: Crew - Scotland's Centre of Expertise for Waters.

Faustini, J. M., & Jones, J. A. (2003). Influence of large woody debris on channel morphology and dynamics in steep, boulder-rich mountain streams, western Cascades, Oregon. *Geomorphology*, *51*(1–3), 187–205. https://doi.org/10.1016/S0169-555X(02)00336-7

Follett, E. (2021). *Dataset: Backwater rise due to jams with a lower gap in an experimental flume*. Zenodo. https://doi.org/10.5281/zenodo.5104958

Follett, E., Schalko, I., & Nepf, H. (2020). Momentum and energy predict the backwater rise generated by a large wood jam. *Geophysical Research Letters*, *47*, e2020GL089346. https://doi.org/10.1029/2020GL089346

Follett, E., & Wilson, C. (2020). Bedload sediment transport induced by channel-spanning instream structures. In *River Flow 2020: Proceedings of the 10th Conference on Fluvial Hydraulics (Delft, Netherlands, 7-10 July 2020)*. London: CRC Press.

Forbes, H., Ball, K., & McLay, F. (2015). *Natural flood management handbook* (Technical Report No. 978-0-85759-024-4). Stirling: Scottish Environment Protection Agency, Strathallan House.

Gallisdorfer, M., Bennett, S., Atkinson, J., Ghaneeizad, S., Brooks, A., Simon, A., & Langendoen, E. (2014). Physical-scale model designs for engineered log jam in rivers. *Journal of Hydro-environment Research*, *8*(2), 115–128. https://doi.org/10.1016/j.jher.2013.10.002

García, M., Laursen, E. M., Michel, C., & Buffington, J. M. (2000). The legend of A.F Shields. *Journal of Hydraulic Engineering*, *126*(9), 718–723. https://doi.org/10.1061/(asce)0733-9429(2000)126:9(718)

Hankin, B., Hewitt, I., Sander, G., Danieli, F., Formetta, G., Kamilova, A., et al. (2020). A risk-based, network analysis of distributed in-stream leaky barriers for flood risk management. *Natural Hazards and Earth System Sciences Discussions*, *20*, 2567–2584. https://doi.org/10.5194/nhess-20-2567-2020

Henderson, F. (1966). *Open channel flow*. Collier MacMillan Publishers.
Hey, R., & Thorne, C. (1986). Stable channels with mobile gravel beds. *Journal of Hydraulic Engineering*, *112*, 671–689. https://doi.org/10.1061/(asce)0733-9429(1986)112:8(671)
Ismail, H., Xu, Y., & Liu, X. (2021). Flow and scour around idealized porous engineered log jam structures. *Journal of Hydraulic Engineering*, *147*, 04020089. https://doi.org/10.1061/(ASCE)HY.1943-7900.0001833
Julien, P. (1998). *Erosion and sedimentation*. Cambridge University Press.
Julien, P. (2010). *Erosion and sedimentation* (2nd ed.). Cambridge University Press.
Keller, E., & Swanson, F. (1979). Effects of large organic material on channel form and fluvial processes. *Earth Surface Processes and Landforms*, *4*, 361–380. https://doi.org/10.1002/esp.3290040406
Leakey, S., Hewett, C. J. M., Glenis, V., & Quinn, P. F. (2020). Modelling the impact of leaky barriers with a 1d Godunov-type schoeme for the shallow water equations. *Water*, *12*(2), 371. https://doi.org/10.3390/w12020371
L'Hommedieu, W., Tullos, D., & Jones, J. (2020). Effects of an engineered log jam on spatial variability of the flow field across submergence depths. *River Research and Applications*, *36*(3), 383–397. https://doi.org/10.1002/rra.3555
Malcherek, A. (2018). Eine neue, auf der impulsbilanz basierende theorie zur hydraulik des schützes – Ein diskussionsbeitrag. *Wasser-Wirtschaft*, *5*, 40–69. https://doi.org/10.1007/s35147-018-0215-8
Manners, R. B., & Doyle, M. W. (2008). A mechanistic model of woody debris jam evolution and its application to wood-based restoration and management. *River Research and Applications*, *24*(8), 1104–1123. https://doi.org/10.1002/rra.1108
Mount, J. F. (1995). *California rivers and streams: The conflict between fluvial processes and land use*. Oakland, CA: University of California Press. https://www.ucpress.edu/book/9780520202504/california-rivers-and-streams
Nakamura, F., & Swanson, F. J. (1994). Distribution of coarse woody debris in a mountain stream, western Cascade Range, Oregon. *Canadian Journal of Forest Research*, *24*, 2395–2403. https://doi.org/10.1139/x94-309
Parker, G., Wilcock, P., Paola, C., Dietrich, W., & Pitlick, J. (2007). Physical basis for quasi-universal relations describing bankfull hydraulic geometry of single-thread gravel bed rivers. *Journal of Geophysical Research*, *112*, F04005. https://doi.org/10.1029/2006JF000549
Persi, E., Petaccia, G., Sibilla, S., Lucía, A., Andreoli, A., & Comiti, F. (2019). Numerical modelling of uncongested wood transport in the Rienz river. *Environmental Fluid Mechanics*, *20*, 539–558. https://doi.org/10.1007/s10652-019-09707-8
Riley, W., Potter, E., Biggs, J., Collins, A., Jarvie, H., Jones, J. I., et al. (2018). Small water bodies in Great Britain and Ireland: Ecosystem function, human-generated degradation, and opportunities for restorative action. *Science of the Total Environment*, *645*, 1598–1616. https://doi.org/10.1016/j.scitotenv.2018.07.243
Roth, A., & Hager, W. H. (1999). Underflow of standard sluice gate. *Experiments in Fluids*, *27*, 339–350. https://doi.org/10.1007/s003480050358
Ruiz Villanueva, V., Bladé Castellet, E., Díez-Herrero, A., Bodoque, J. M., & Sánchez-Juny, M. (2014). Two-dimensional modelling of large wood transport during flash floods. *Earth Surface Processes and Landforms*, *39*(4), 438–449. https://doi.org/10.1002/esp.3456
Schalko, I., Schmocker, L., Weitbrecht, V., & Boes, R. M. (2018). Backwater rise due to large wood accumulations. *Journal of Hydraulic Engineering*, *144*(9), 04018056. https://doi.org/10.1061/(ASCE)HY.1943-7900.0001501
Schalko, I., Wohl, E., & Nepf, H. (2021). Flow and wake characteristics associated with large wood to inform river restoration. *Scientific Reports*, *11*, 86644. https://doi.org/10.1038/s41598-021-87892-7
Shields, F. D., & Gippel, C. J. (1995). Prediction of the effect of woody debris removal on flow resistance. *Journal of Hydraulic Engineering*, *121*(4), 341–354. https://doi.org/10.1061/(asce)0733-9429(1995)121:4(341)
Wallerstein, N., & Thorne, C. (1996). Technical Report No. WK2Q6C-8096-EN09. Impacts of woody debris on fluvial processes and channel morphology in stable and unstable streams. In *US Army Research Development & Standardization Group*. (Vol. ADA286933. London: U.S. Army Corps of Engineers. https://apps.dtic.mil/sti/citations/ADA286933
Wohl, E., Angermeier, P. L., Bledsoe, B., Kondolf, G. M., MacDonnell, L., Merritt, D. M., et al. (2005). River restoration. *Water Resources Research*, *41*(10), W10301. https://doi.org/10.1029/2005WR003985
Wohl, E., Bledsoe, B. P., Fausch, K. D., Kramer, N., Bestgen, K. R., & Gooseff, M. N. (2016). Management of large wood in streams: An overview and proposed framework for hazard evaluation. *Journal of the American Water Resources Association*, *52*(2), 315–335. https://doi.org/10.1111/1752-1688.12388
Wohl, E., & Jaeger, K. (2009). A conceptual model for the longitudinal distribution of wood in mountain streams. *Earth Surface Processes and Landforms*, *34*(3), 329–344. https://doi.org/10.1002/esp.1722